



# Quantum computing with Rydberg atom graphs

Minhyuk Kim<sup>1</sup> · Jaewook Ahn<sup>1</sup> · Yunheung Song<sup>2</sup> · Jongchul Moon<sup>2</sup> · Heejeong Jeong<sup>3</sup>

Received: 30 September 2022 / Accepted: 29 October 2022 / Published online: 13 March 2023  
© The Korean Physical Society 2023

## Abstract

In recent years, Rydberg atom graphs, which are the arrangement of atoms of which the interaction through Rydberg state excitation can be represented by a mathematical graph, have emerged as a promising qubit platform for quantum computing and quantum simulation, through implementing quantum gates and circuits, probing quantum phase transitions in designed atom arrays, and solving the classically difficult class of computational problems. Here we briefly review the remarkable progress of the related techniques and research activities involved with the Rydberg atom graphs. The ease of scalability and controllability of Rydberg atom graphs might enable the quantum advantage in the NISQ (noisy intermediate scale quantum) era.

**Keywords** Rydberg atom · Quantum computing · Quantum simulation

## 1 Introduction

During the last decade, there have been two breakthrough technologies which have played essential and respective roles in Rydberg quantum computing research, impacting on the current remarkable progress of the field. The first is the Rydberg blockade effect [1–3], which has made the entanglement of neutral atoms an everyday tool in the worldwide atomic quantum research, and the second is the atom rearrangement method [4–6], which utilizes a set of movable optical tweezers to construct defect-free arbitrary atom graphs, as in Fig. 1. Here we use the term Rydberg atom graphs, because possible geometries of as-constructed atom arrays are not limited to crystalline structures in the physical, three-dimensional space, but are better represented by mathematical graphs, which are the set of vertices and edges in hyper-geometric space. In that regard, Rydberg atom systems of the general form can be referred to as Rydberg atom graphs (or Rydberg graphs, in short).

Rydberg atoms are a micrometer-size neutral atom of a large principal quantum number (about  $n = 100$ ). The interaction between two Rydberg atoms, e.g., in  $10 \mu\text{m}$  distance, is huge, about  $10^{13}$  times stronger than the interaction between two ground-state ( $n = 1$ ) atoms at the same distance, due to the large polarizability of Rydberg atoms. As a result, the presence of a Rydberg atom easily prohibits neighboring ground-state atoms from becoming Rydberg atoms. Simultaneous creation of Rydberg atoms within a certain distance (Rydberg blockade distance, about  $10 \mu\text{m}$  for  $n = 100$ ) results in a quantum mechanically entangled many-body state. The strong interaction of Rydberg atoms also makes fast quantum gates (of up to MHz clock speed).

Rydberg quantum computers use a Rydberg atom graph and controls its many-body entanglement nature, to compute classically difficult quantum or classical problems by either performing quantum simulation, adiabatic quantum computing, or circuit-based quantum computing. The atoms are individually controlled sequentially or simultaneously by lasers or RF fields, so that the multi-partite quantum entanglement state of the atoms can be altered according to a prepared quantum algorithm. In particular, the placement and movement of individual atoms are relatively easy in Rydberg atom experiments, i.e., Rydberg atoms are non-stationary qubits allowing adjustable qubit couplings presumably even during quantum computing process. It is possible to implement arbitrary Rydberg graphs, or equivalently arbitrary qubit connections required for combinatorial optimization problems in adiabatic quantum computing. The versatility of

✉ Jaewook Ahn  
jwahn@kaist.ac.kr

<sup>1</sup> Department of Physics, KAIST, Daejeon 34141, Republic of Korea

<sup>2</sup> Korea Research Institute of Standards and Science, Daejeon 34113, Republic of Korea

<sup>3</sup> Q Center, Sungkyunkwan University, Suwon 16419, Republic of Korea

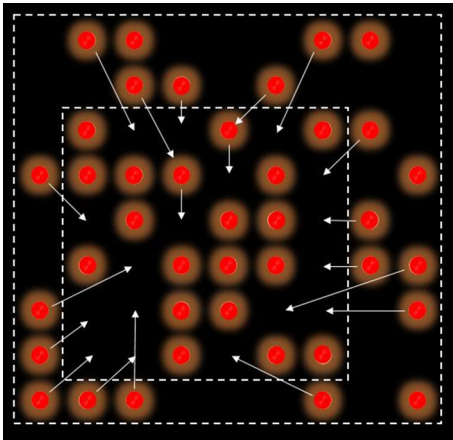


**Fig. 1** Illustration of atom rearrangement: A small-size defect-free atom array is constructed from a large-size probabilistically occupied atom array by simultaneous or sequential atom rearrangement [4–6]

Rydberg atom graphs has enabled significant research progress of Rydberg atom quantum computing in recent years.

This review focuses on the recent progress of the Rydberg quantum computations and simulations, in addition to the previous reviews [7–12]. To begin, we briefly introduce the Rydberg atom quantum computer. We then review the technical details to realize universal Rydberg quantum gate operations, quantum simulation, and finally quantum adiabatic computing with Rydberg atom graphs. We discuss the prospects of Rydberg quantum computing in the end.

## 2 Rydberg atom quantum computer

A Rydberg atom quantum computer consists of a single-atom apparatus, atom rearrangement system, a Rydberg excitation laser system, and a state measurement apparatus.

### 2.1 Single atom apparatus

A magneto-optical trap (MOT) is used to prepare cold atoms. Fast-moving atoms at the room temperature are made to be stationary in a vacuum space. The atom speed is reduced from 1000 m/s to 0.1 m/s or less, and the temperature (or the speed distribution) is lowered down to 0.01 mK. Up on being irradiated by near-resonant (red-detuned) laser light, the atoms moving toward the irradiation lose their momentum through a repetitive process of directional absorption and isotropic spontaneous emission. Such an optical molasses process eventually stops the atoms in a spatial trap potential determined by an anti-Helmholtz magnetic field.

Optical dipole traps (or optical tweezers, hereafter) are used to prepare single atoms [6, 13–18]. Light-induced energy shift (the AC Stark shift) of the atoms can be either

positive or negative from the the atomic resonance according to the detuning of the light frequency. Red-detuned light (below the resonance) creates an attractive optical potential for the atoms by down-shifting the ground state energy level and up-shifting the excited state energy level. So, typical optical tweezers use red-detuned laser light to trap the atoms using a tightly focused laser beam, of which laser frequency is tuned far off from the atomic resonance so that the trapped atoms nearly do not absorb the light and preserve their internal energy state. At a proper condition laser intensity and beam diameter, single or no atom occupancy in a trap is provided by the collisional blockade condition [24].

While Rydberg single-atom experiments mostly use red-detuned optical tweezers due to the simplicity and efficiency, blue-detuned optical field can be also used to confine the atoms [18]. In this case, the at the light intensity minimum, by surrounding the atoms by repulsive potentials induced by higher intensities of the blue-detuned trap laser [17, 20–23]. The intensity distribution of blue-detuned optical dipole traps can be a Laguerre–Gaussian type or bottle-beam traps. The use of the blue-detuned trap resolves the disadvantage of the red-detuned optical tweezers, the ponderomotive potential [20], which prohibits Rydberg atoms from being trapped by the red-detuned optical tweezers. While red-detuned optical tweezers must be turned off during the Rydberg excitation to avoid the anti-trapping, the blue-detuned traps can be kept on. So, the blue-detuned “dark” traps are likely provide longer time (than red-detuned ones) in quantum simulation and high-fidelity gate operations [21]. Three-dimensional trapping of an individual Rydberg atom is demonstrated by bottle beam traps formed by a holographic spatial light modulator [22] and a larger dark trap array of more than 1,000 atoms has been demonstrated with a passive mask and spatial filtering [23], showing the possibility of large-scale Rydberg trapping in future.

### 2.2 Atom rearrangement system

An atom-rearrangement system provides a defect-free atom array or graph, of which the process consists of three steps: atom occupancy check, atom-moving path design, and atom transport. Without the atom rearrangement, each lattice point of an array of  $2N$  optical tweezers is probabilistically half-filled, i.e., only about  $N$  optical tweezers hold single atoms and remaining optical tweezers have no atoms, as illustrated in Fig 1. It is because the atoms captured by an optical tweezer escape from the trap by pair-wise collisions, due to the collisional blockade effect [24] and at a certain trap beam-width and potential condition, the number of atoms is either 1 or 0, so the probability of capturing a single atom is about 0.5.

The atom rearrangement for a perfectly occupied (defect-free)  $N$ -atom array begins with a stochastically loaded  $2N$ -atom array, which is changed to a defect-free one by moving the loaded single atoms individually. The optical tweezers that capture atoms are to be moved to form a desired atom arrangement close to a deterministic probability,  $\langle N \rangle = 1$ . For this purpose, a liquid-crystal type spatial-light-modulator (LC-SLM) or an acousto-optic deflector (AOD) is used to create and move multiple laser beams at a high speed. As such, defect-free atom arrays are generated by dynamically rearranging optical tweezers. The laser beam can be separated to place 20–250 atoms on to a two- or three-dimensional spatial arrangement. The quality of the array is directly related to the uniformity of the individual potential depths of the optical tweezers. And the uniformity can be maintained to be of high quality by aberration compensation and also by modifying hologram calculating algorithm [25–28]. The methods of generating trap arrays include holographic [15], acousto-optic methods [6], and microlens array [16].

**Holographic method:** The holographic method uses computer-controlled liquid-crystal spatial-light modulators (LC-SLM). It modulates the spatial phase of an incident reference laser beam. An appropriate phase mask programmed on the LC-SLM renders the desired intensity distribution of the array. The Gerchberg–Saxton (GS) algorithm is widely used to find the phase mask with the best efficiency and uniformity. It is iterative Fourier- and inverse-Fourier-transform between a reference electric field  $A(x, y)e^{i\Phi(x, y)}$  in the Fourier-plane  $(x, y)$  and a desired target intensity distribution  $I(x', y', z')$  in the image space  $(x', y', z')$  until the former converges to the latter so that a desired intensity distribution is shaped from the initial random phase pattern [15].

However, when the GS algorithm generates each movie frame of the phase mask for atom rearrangement, the transition phase between two consecutive phases shows a significant flicker of trap intensities due to phase discontinuity, resulting in the loss of atoms. KAIST group demonstrated the first simultaneous rearrangement of single atoms by implementing a dynamic holographic phase mask with a flicker-free beam steering algorithm [4]. An LC-SLM shapes the wave front of a laser beam to form a designed array simultaneously. The hologram calculation algorithm was optimized to prepare dozens of two-dimensional defect-free atomic arrays. Without the method of atom rearrangement, the simultaneous capturing of  $N$  atoms has a low probability of  $1/2^N$ . For example, capturing ten atoms with ten optical dipole traps usually results in a random capture of 4–6 atoms, and capturing all ten atoms results in a small probability of about 0.001. The atom rearrangement method resolves this problem and enables capturing defect-free  $\langle N \rangle$  atoms at a high probability near one.

The GS algorithm has been further advanced by applying the Hungarian matching algorithm [29] and modifying Gerchberg–Saxton algorithm [30]. For example, zero-padding is added to the Gerchberg–Saxton algorithm to increase the position resolution of the optical trap in the Fourier transform (Fig. 2a). In addition, weights and induction are added for faster convergence of each frame and phase continuity between successive frames, respectively, resulting in reduced flicker and improved agility. To minimize the atomic movement path and prevent collisions between the paths, a movement path is given between the first captured atom and the uncaught optical traps using the Hungarian algorithm (Fig. 2b). The hologram can be calculated at a 60 Hz repetition rate using a GPU, and typically 15 to 20 frames are required to rearrange the atoms. This feedback is repeated nine times to create a defect-free array of more than 30 atoms within 2 s. Figure 2b is an example of preparing a butterfly-shaped flawless array of 37 atoms with a probability of about 35%. Later, 49 neutral atoms were successfully relocated to a three-dimensional space using an improved technique that minimizes interference [31]. A dynamically programmed LC-SLM hologram device reflected a laser beam to create  $2N$  position-controllable optical tweezers, and  $N$  rubidium atoms were relocated in a three-dimensional space.

**Acousto-optic method:** Groups in Harvard and Institut d’Optique respectively developed sequential one-by-one atom transportation by deploying about 100 neutral atoms

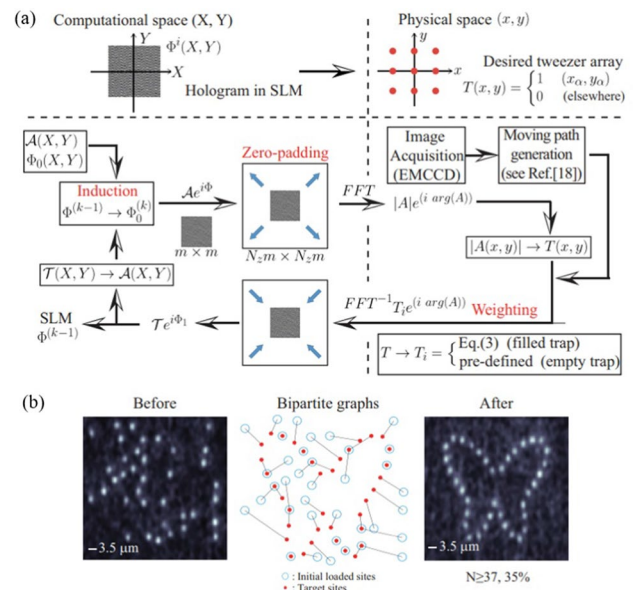


**Fig. 2** Defect-free atomic array generation using holographic method. **a** Entire block diagram of the modified Gerchberg–Saxton algorithm for atom rearrangement. **b** An example of preparing a butterfly-shaped array of 37 atoms with a probability of about 35%. Reprinted with permission from [30] ©The Optical Society

using acousto-optic deflectors (AOD) [5, 6]. Currently, up to 250 atoms are spatially placed and used for quantum simulation or quantum computing research. The acousto-optic method also generates optical tweezer arrays. When the radio-frequency (RF) wave is sent to the acousto-optic modulator or deflector (AOM or AOD), a portion of the incident light is deflected by the angle corresponding to the RF frequency. The number of deflected beams corresponds to the frequency components of RF, and the deflection angles correspond to the values of frequencies [6].

Unlike KAIST's approach, the AOD method differently shuttles each atom. The first step is to create  $2N$  two-dimensional lattice-shaped optical traps using spatial-light-modulator (SLM), then determine the positions of about  $N$  neutral atoms captured with a 50% stochastic probability. An additional moving tweezer diffracted from a 2d-acousto-optic-deflector (2d-AOD) is superimposed on a trap beam modulated by SLM. By moving the identified atoms one by one in the XY direction using two AODs driven at high speed, they generated  $N$  atomic arrays of the desired shape. The position and intensity of the moving tweezer are controlled by the frequency and amplitude of the input RF wave applied to the 2d-AOD [5], as in Fig. 3(a). The depth of the moving tweezer becomes deeper than the overlapped SLM trap, and the trapped atom initially in the SLM trap is transferred to the moving tweezer. Then the tweezer moves to another SLM trap site with a typical speed of  $10 \text{ nm}/\mu\text{s}$ , as shown in Fig. 3(b). So, it takes about 1 ms for  $10 \mu\text{m}$  movement per single atom. Figure 3(c) demonstrates 25 atoms defect-free array generation, where the average filling fraction is increased from 50% to 96%. With a 96% chance of success, they made square arrays of 25 neutral atoms. At this time, the travel time for each atom takes 1 ms per 10 micrometers of the atom interval, limiting the maximum number of atoms that can be placed to hundreds. It is also applicable to generate multiple moving tweezers with multi-frequency RF [6]. The sequential one-by-one technique has been advanced in

assignment algorithms [32, 33], and hybridizing a partially parallel technique for their 256-qubit processor [34]. The rearrangement for the three-dimensional array has also been demonstrated [31, 35].

*Other methods:* There are many other different methods available for atom rearrangements, one of which is the microlens array, which explicitly divides the incident light into the array of focus spots [16], and the other is the bottle-beam trap array, which uses a diffractive beam splitter and calcite displacers [17].

### 2.3 Rydberg excitation

Once a defect-free Rydberg-atom graph is prepared, Rydberg excitation is usually the next stage [36]. Rydberg atoms are created using a laser or lasers through a one- or two-photon absorption process. Required lasers are to have a narrow line width (less than 10 kHz), which is often achieved by frequency stabilizing with a Fabry-Perot resonator (typically 100 kHz line width). In addition, it is known that laser phase noises from servo bumps of frequency locking are one of the major sources of imperfections in Rydberg excitation [37], so cavity-filtered diode lasers [38] or Ti:Sapphire lasers are used for a better quality of the excitation.

### 2.4 State measurement

The final stage is to measure whether an atom is in the ground state or in the Rydberg state. The measurement utilizes the fluorescence imaging to check the presence of an atom in each trap with a high-sensitivity camera (mainly using an electron amplification camera, an EMCCD, or a scientific CMOS camera). Since Rydberg atoms are not trapped by tweezer traps, the Rydberg (ground) state can be mapped into absence (presence) in the trap with fidelity over 90% [37]. Rydberg ionization by microwave can be used for better fidelity, especially in blue-detuned traps [39].

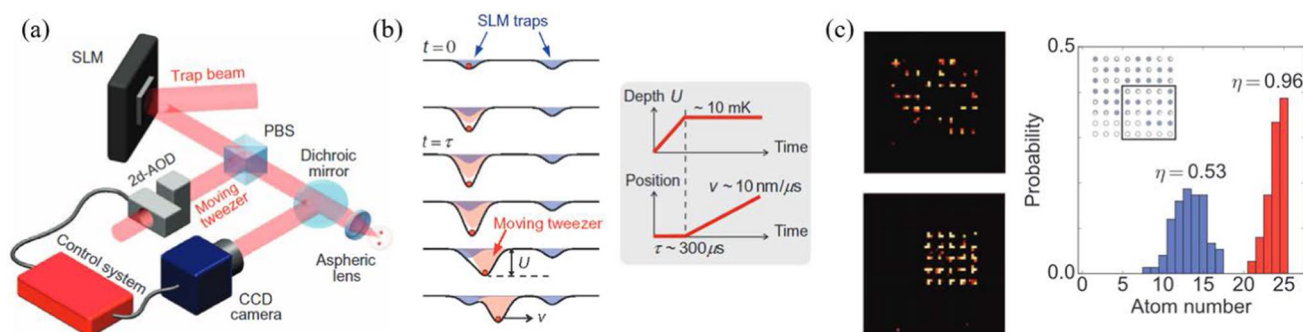


**Fig. 3** Defect-free atomic array generation using acousto-optic method. **a** Experimental setup. **b** Atomic shuttling scheme by a moving tweezer diffracted from the 2d-AOD. **c** Demonstration of generat-

ing a defect-free array of  $5 \times 5$  square lattice. Reprinted figure from [5] with permission from AAAS

Transferring a Rydberg state into a ground hyperfine state [40] is also used for state measurement with selective hyperfine state detection [41–43], especially when multiple Rydberg states are used [44].

### 3 Quantum computing

#### 3.1 Manipulating entangled states

While the entangled state of Rydberg atoms utilizing Rydberg blockade [1, 45] remained as a theoretical idea for a while, experimental demonstrations were finally achieved with two atoms [40, 46] or atomic ensemble [47]. Rydberg dressing-based entanglement generation was demonstrated [48], but it was also based on a blockade mechanism for two atoms. After the rearrangement technique became available, Rydberg-mediated many-body entanglement states of a large deterministic atom array have become available, utilizing the high degree of freedom and flexible shapes of Rydberg atom graphs.

The first manipulation of Rydberg atom entangling gates was realized in a weak interaction regime, where the Rydberg atoms are spaced far beyond the Rydberg blockade distance [49]. The Rydberg phase gate is based on a phase induced by Rydberg–Rydberg interaction resulting in a controlled Z gate, and then probed by the Ramsey interferometry technique, as in Fig. 4(a). Note that this gate can be applied even when nearby atoms are closer than the target atom, keeping nearby atoms non-entangled (Fig. 4b–e). The basic principle of this scheme

was originally proposed as model A in Ref [45], which could not draw much attention due to the sensitivity to the distance between atoms. Neutral atom optical tweezer platforms can minimize a distance error per unit distance by arbitrarily changing the distance while fixing the unit distance error. As a result, the interaction noise can be suppressed between qubits because the interaction (proportional to  $d^{-6}$ ) between qubits is a function of distance  $d$ . In Rydberg quantum computing, the distance error is usually tens of nanometers at a distance of 10 micrometers, making interaction noise as small as 1/1000. This advantage enables a long-distance Rydberg quantum gate operation in addition to the conventional Rydberg quantum computing based on the Rydberg blockade phenomenon among the nearest neighbors.

The generation of a multi-qubit entangled state called the Greenberger–Horne–Zeilinger (GHZ) state has also been demonstrated. In Rydberg atom arrays, the many-body W-type entangled states can be directly generated using the Rydberg blockade effect. Generating another type of entangled state, GHZ-states, or Schrödinger cat states, has been of particular interest. Such states are considered as standard states to benchmark the performance of a quantum processor due to their fragility. Utilizing natural Ising-like interaction in one dimensional Rydberg atom array and local energy control by Stark shift laser beams, GHZ states up to 20 qubits of ground-Rydberg states were prepared and manipulated by quasi adiabatic evolution as in Fig. 4(f–h) [50]. This was the largest GHZ state generation at that time, showing the competitiveness of neutral-atom platforms compared with other platforms [51–53].

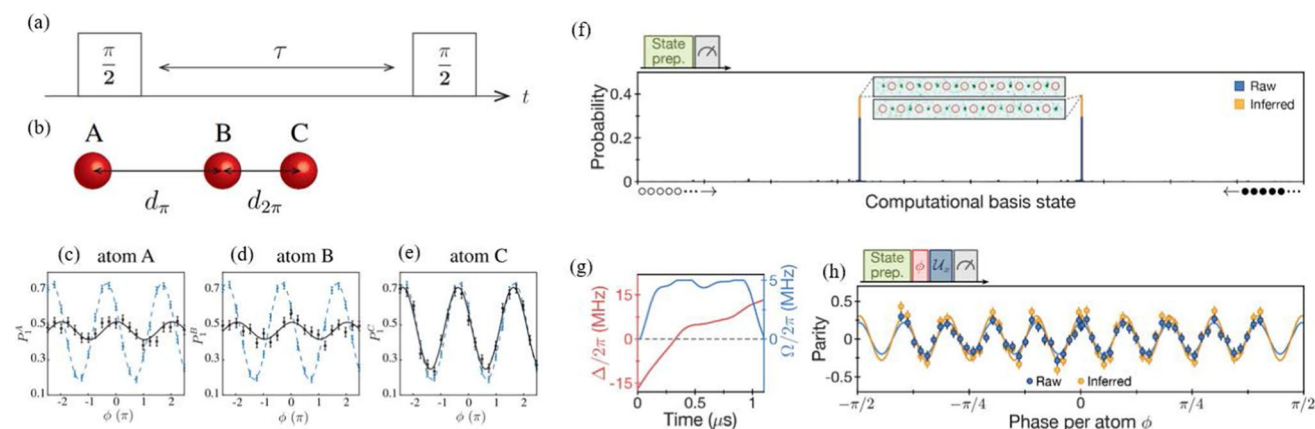


**Fig. 4** Manipulating entangled state by Rydberg atoms. **a** A Ramsey-type phase gate induced by Rydberg atom interaction. **b** Linear arrangement of three atoms A, B, C with inter-atomic distances  $d_{AB} = d_{\pi}$  and  $d_{BC} = d_{2\pi}$  giving  $\pi$ - and  $2\pi$ - phases, respectively. **c** Measured Ramsey-fringes  $P_1(\phi)$  of (c) atom A, **d** atom B, and **e** atom C, showing that atoms A and B are entangled. **f** An experimen-

tal probability histogram of computational basis micro-states for 20 atoms, showing the GHZ state. **g** Pulse parameters for preparing the GHZ state. **h** Parity oscillations between GHZ state components. **a–e** from [49], reprinted with permission. **f–h** from [50], reprinted with permission from AAAS

### 3.2 Quantum gates and circuits

Atomic hyperfine-state pair is one of the promising candidates for qubit encoding thanks to its high coherence, which can be used for frequency standards. Many quantum processors are based on quantum gates, designed unitary evolution of a single qubit or multi-qubits, so high atomic state controllability is required. Especially, circuit-model quantum computation relies on universal quantum gate sets, which can be constructed by arbitrary single-qubit and two-qubit gates. Single-qubit gates implemented by global microwaves and local laser beams have been well established in 2D [54] and 3D [55] without deterministic atom arrays, showing high fidelity over 99%. With the tweezer array platform, single-qubit gates were proposed and demonstrated based on geometric phases induced by ultrafast laser pulses in picosecond time scale [56] and Raman lasers generated by a dispersive optical system [57].

For two-qubit gates, since the first demonstration of Rydberg-mediated entanglement of atomic qubits [40, 46], there have been many efforts to achieve high-fidelity entanglement for about a decade. Standard gate scheme [45] and Rydberg dressing [48] were tested, failing to achieve a high fidelity over 90%. But, after analyzing [37] and resolving [38] the imperfect Rydberg excitations issue, high fidelity CZ gate of about 97% has been achieved by a new gate scheme, which utilizes Rydberg blockade and geometric phase induced by two Rydberg pulses, the so-called “Levine-Pichler” gate [58] (See Fig. 5). This symmetric global gate is faster and experimentally simpler than the standard gate scheme that requires single-site addressing [39], so it is frequently used for Rydberg-mediated entanglement as a new standard. The implementation of three-qubit Toffoli gates is also demonstrated in the same paper, which may improve circuit depth requirements. The current fidelity is still insufficient for both NISQ and fault-tolerant quantum applications. The limitation is not intrinsic but technical, so further fidelity improvement is expected shortly. Some single-pulse symmetric schemes by pulse shaping are proposed [59–61] and demonstrated [62], and these could boost the improvement of Rydberg entangling gates.

Most recently, neutral-atom quantum processors have become capable of implementing quantum circuits in programmable and complementary manners [63, 64] (See Fig. 6). Authors of Ref. [63] use a globally addressed laser beam for Rydberg excitations and coherent atom transports in the middle of circuits to implement CZ gate programmability. It utilizes the locality of Rydberg interaction which decays rapidly. This method can generate geometrical connectivity in two-dimensional planes and torus surfaces to implement the toric code. It can be also used for various applications such as mid-circuit measurements and quantum simulation. However, it has a disadvantage of the transport

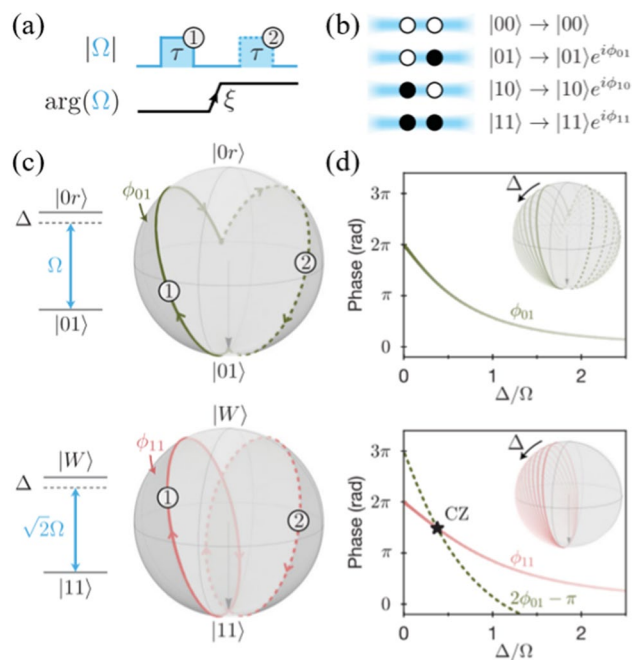


**Fig. 5** Quantum gates on Rydberg atom systems. **a** Controlled phase gate protocol. Two pulses with detuning  $\Delta$  and Rabi frequency  $\Omega$  are globally addressed with different phases  $\xi$ . **b** The results of the protocol for different basis states. The dynamic phases are accumulated except for  $|00\rangle$ . **c** Bloch sphere illustrations of the state’s evolution by the controlled phase gate. The pulse duration  $\tau$  and phase jump  $\xi$  are chosen so that the initial states  $|01\rangle$  and  $|10\rangle$  undergo a single complete oscillation,  $|11\rangle$  undergoes two complete oscillations. **d** The detuning  $\Delta$  is chosen to satisfy a relation between the dynamical phases  $\phi_{11} = 2\phi_{01} - \pi$  to implement the controlled phase gate protocol. Reprinted figures with permission from [58]

speed to take up to hundreds of microseconds of circuit programming time.

The other processor of six qubits [64] uses a complementary scheme for quantum circuit programming with tightly focused Rydberg lasers to locally address atomic qubits, maintaining high CZ fidelity. Its high gate clock speed ( $< 10$  us) allows quantum circuit implementation, such as GHZ state preparation, quantum phase estimation (QPE), and quantum approximate optimization algorithm (QAOA), up to 18 CZ gates despite a few ms coherence time without dynamical decoupling. Combining two schemes will make the neutral-atom quantum platform more attractive for quantum information processing with a unique capability differentiated from other platforms.

### 3.3 Quantum simulations

Due to the advantage of scalability, programmable Rydberg atom arrays are considered as a good platform for quantum simulation [65, 66], which explores quantum phenomena of strongly correlated many-body systems based on

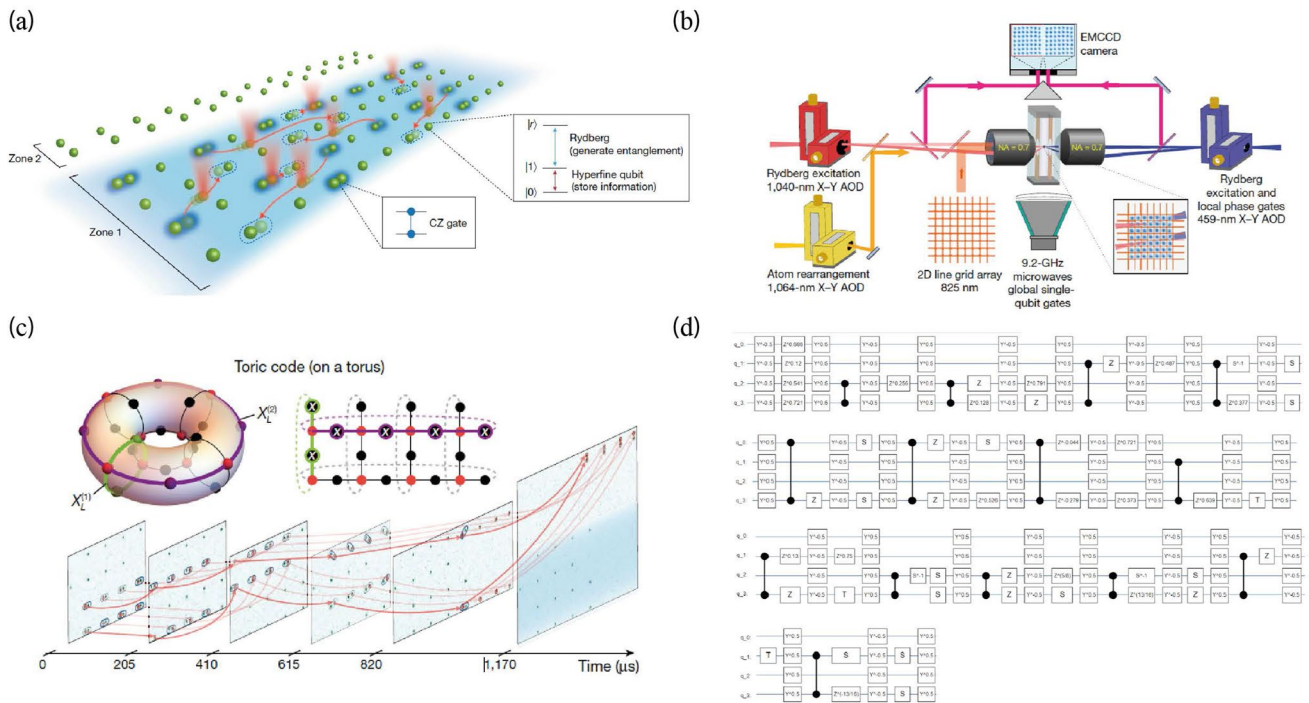


**Fig. 6** Quantum circuit programming on Rydberg atom systems by (a) coherent transport of entangled atom arrays and b universal gate set implemented by tightly focused lasers and global microwaves. c Implementing the toric code by sequential movements of ancilla

qubits. d Quantum circuit of the quantum phase estimation for hydrogen molecular energy, decomposed by the native gate set. a, c Reprinted figures from [63], b, d from [64]

microscopic observations. In quantum simulation, individually trapped atoms act as pseudo-spins in which the atomic Rydberg and ground states are mapped to spin up and down,  $|\uparrow\rangle$  and  $|\downarrow\rangle$ , respectively, so that the system where the neighboring atoms interact with each other via Rydberg blockade can be expressed as the quantum Ising Hamiltonian [67]:

$$H(t) = \sum_{i<j} U_{ij} n_i n_j + \frac{\hbar\Omega(t)}{2} \sum_i \sigma_i^x - \hbar\delta(t) \sum_i n_i, \quad (1)$$

where  $U_{ij}$  is van der Waals interaction proportional to  $1/R_{ij}^6$  for an inter-atomic distance between atoms  $i$  and  $j$  [68],  $n_i = |\uparrow\rangle\langle\uparrow|_i$ ,  $\sigma_i$  are the Pauli matrices,  $\Omega$  is laser Rabi frequency coupling  $|\downarrow\rangle$  and  $|\uparrow\rangle$ , and  $\delta$  is laser detuning.

A simple experimental implementation is to observe quench dynamics; which suddenly turns on a constant transverse field  $\hbar\Omega\sigma^x/2$  to a system. A result of quench dynamics for a super-atom of  $N$ -atoms, where all atoms are in a single Rydberg blockade range, is a collective Rabi-flopping between a ground state  $|\downarrow\downarrow\downarrow \dots\rangle$  and the W-state  $(|\uparrow\downarrow\downarrow \dots\rangle + \dots + |\downarrow\downarrow\downarrow \dots\rangle)/\sqrt{N}$  with the frequency  $\sqrt{N}\Omega$  [67]. The many-body dynamics with more interacting connections result from the sum of the couplings between various eigenstates of the Hamiltonian Eq. (1) restricted by the Rydberg blockade effect. The change of such many-body eigenstates is observed by transforming the connected

graph structures of atoms arranged in three-dimensional space [69]. The many-body quench dynamics of atomic arrays with more than 10 qubits show diffusive properties along the Hamiltonian eigenstates corresponding to Fibonacci graphs explained by the Fokker–Planck classical diffusion model [70].

Another experimental implementation is quantum annealing, a technique that slowly adjusts the Hamiltonian of a many-body quantum system to transform an initial state that is easy to make into a desired final state. This is a protocol to simulate quantum phase transitions between two different magnetic phases [71]. In particular, if the Hamiltonian passes near the quantum phase transition during the quantum annealing process, it performs a quantum computing task requiring an energy comparison between many-body entanglement states. A typical experimental sequence is illustrated in Fig. 7(a). Initially all atoms are prepared to paramagnetic (PM) states  $|\downarrow\downarrow \dots\rangle$ , which is the ground state of  $H(t=0)$  at  $\delta(t=0) < 0$ . Then the Hamiltonian  $H(t)$  evolves by turning on and off the laser Rabi frequency  $\Omega(t)$  and increasing the detuning  $\delta(t)$  to  $0 < \delta(t_f) < U$  at final time  $t_f$ , where  $U$  is nearest-neighbor interaction strength. Finally the system evolves to antiferromagnetic (AF) ground state  $|\uparrow\downarrow\downarrow \dots\rangle$  of  $H(t_f)$ . Such experiments have been conducted in atomic arrays in 1D [72], 2D [34, 73, 74], and 3D fractal structures [75].

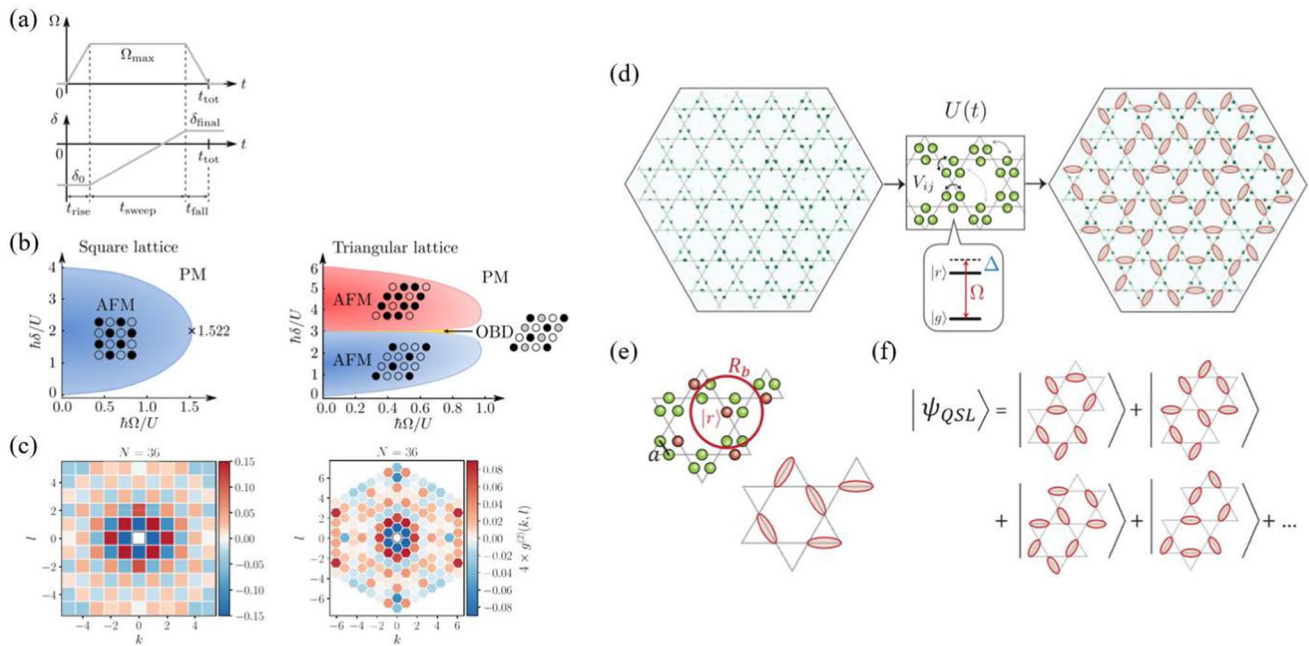


**Fig. 7** Quantum simulation of magnetism on Rydberg atom arrays. **a** Typical experimental sequence. **b** Phase diagram of square and triangular lattices with 36 atoms. **c** Antiferromagnetic correlations of square and triangular lattices. **d** Quantum phase transition of a kagome lattice with 219 atoms from paramagnet to quantum spin liquid (QSL) phase. **e** Tuning Rydberg blockade radius  $R_b$  to for 1/4 excitation filling phase. **f** QSL state is ideally a coherent superposition of exponential dimerized configurations. **a–c** Reprinted figures from [73]. **d–f** Reprinted figures from [77] with permission from AAAS

Recently, several quantum phase transitions between two different magnetic phases have been simulated on two-dimensional arrays of more than 100 atoms [34, 74] with several technical improvements [28, 32]. Two types of geometries, a  $14 \times 14$  square array and a 147-atom triangular array, are tested for the transition to two sublattices and 1/3 filling phases, respectively. From the probability distributions of their microscopic spin configurations, quantitative analysis is conducted by calculating some observables such as the staggered magnetization and the connected spin–spin correlation functions [74]. The antiferromagnetic correlations grow differently by the Hamiltonian sweep rate according to the quantum Kibble–Zurek mechanism [76]. And it is shown that the correlations follow the universal behavior of the Ising quantum phase transition that is theoretically predicted before [34].

Preparation and detection of a quantum spin liquid (QSL) in a Rydberg quantum simulator is also recently reported [77]. QSL, explained by topological order with many degenerate ground states [78], draws much attention due to its application for protected quantum information processing [79]. A Rydberg atom array of up to 219 atoms on the edges of the kagome lattice implements dimer bond models for each vertex. The Rydberg-blockade Hamiltonian is tuned to about 1/4 filling to achieve the exponential number of degenerate dimer coverings of a ground state, as in Fig. 7(d–e). Such enormous dimer configurations reconstruct

a QSL quantum state  $|\psi_{QSL}\rangle$ , which is ideally a coherent superposition of dimer coverings in Fig. 7(f). Then, by adding a hole in the lattice, the topological properties of two distinct topological sectors are used as a logical qubit, a candidate application for quantum information processing in a more elaborate experimental device in future.

Dynamics of quantum many-body systems and non-equilibrium phenomena are very difficult to simulate in digital electronic computers and remain a challenge to be resolved [80]. Due to thermalization from chaotic dynamical behavior, controlling the dynamics is also very hard. And few examples of avoiding thermalizations are known, such as many-body localization [81] and quantum many-body scar [82]. The quantum many-body scar in a two-dimensional Rydberg array of up to 200 atoms is experimentally shown by observing dynamics of highly nonergodic coherent oscillation between ordered and disordered states after quenching Hamiltonian that follows the preparation of the ordered ground state [83]. In addition, a new stabilization phenomenon of the coherent oscillation by periodic driving, which reminds discrete time crystal [84], is also demonstrated and expected to be used for quantum information science.

Resonant dipole–dipole interactions between Rydberg atoms can be applied to program different types of Hamiltonian other than the Ising model. Two atoms prepared as

different Rydberg states  $|r\rangle$  and  $|r'\rangle$  are coupled by a microwave transition. Their dipolar interaction induces population exchange between Rydberg pair states  $|r, r'\rangle$  and  $|r', r\rangle$ . Here each Rydberg states are mapped to a spin-1/2 states  $|\uparrow\rangle \equiv |r\rangle$ ,  $|\downarrow\rangle \equiv |r'\rangle$ . For an inter-atomic distance  $R$ , the interaction strength scales at  $\sim 1/R^3$ . The Hamiltonian of this system is expressed by XY-model:

$$H_{XY} = \sum_{i \neq j} \frac{C_3}{R_{ij}^3} (\sigma_+^i \sigma_-^j + \sigma_-^i \sigma_+^j) \quad (2)$$

where  $C_3$  is a coefficient of the interaction, and  $\sigma_{\pm} = \sigma_x \pm i\sigma_y$ . A three-atom linear chain system is initially prepared to a state  $|\uparrow\downarrow\downarrow\rangle$  for the case of first atom excitation only. The excitation is transferred to the adjacent atoms. Then the spin excitation hopping occurs between each atoms, as  $|\uparrow\downarrow\downarrow\rangle \rightarrow |\downarrow\uparrow\downarrow\rangle \rightarrow |\downarrow\downarrow\uparrow\rangle \rightarrow |\downarrow\uparrow\downarrow\rangle \rightarrow |\uparrow\downarrow\downarrow\rangle$  [85, 86]. Recently, the Hamiltonian in Eq. (2) has been applied to study the topological states of matter. An atomic array of zig-zag chains encodes the repeating angular-dependent strong ( $J$ ) and weak ( $J'$ ) interactions between odd and even lattice sites. Such an array implements the Su–Schrieffer–Heeger (SSH) model describing a one-dimensional dimerized chain, in which the finite lattice can behave as a topological insulator [87].

Combining an engineered microwave illumination and Rydberg atoms with exchange interactions can implement the Heisenberg spin model. In Ref. [88], a sequence of four  $\pi/2$  microwave pulses couples two different Rydberg states  $|r\rangle$  and  $|r'\rangle$  to implement the Hamiltonian expressed by:

$$H_{Heisenberg} = \frac{1}{2} \sum_{i \neq j} J_{ij}^x \sigma_x^i \sigma_x^j + J_{ij}^y \sigma_y^i \sigma_y^j + J_{ij}^z \sigma_z^i \sigma_z^j, \quad (3)$$

where the interaction strengths  $J_{ij}^{x,y,z}$  are changed by the delay times of the microwave pulses.

### 3.4 Combinatorial optimization problems

The NP (non-deterministic polynomial) problems are the problems with a high computational complexity that current digital computers of von Neumann architectures are difficult to deal with. The decision problems are classified into P (deterministic polynomial) and NP according to the computational complexity, among which the NP-problems cannot be efficiently solved using digital computer algorithms. The challenge of the currently developing quantum computers is to efficiently (i.e., in a polynomial time) solve NP-problems such as quantum Fourier transforms (QFT) in factorization problems. Especially, NP-complete problems draw attention due to their reducibility from all P and NP problems. Maximum-independent-set problem, 3-satisfiability (SAT)

problem, and most combinatorial optimization problems belong to the class of NP-complete problems.

Rydberg atom arrays can intrinsically access some NP-complete combinatorial optimization problems such as maximum-cut [64] and maximum-independent-set (MIS) problems [89–91] of given graphs  $G(V, E)$ . The individual atoms are mapped to vertices  $V$ . Edges  $E$  maps the nearest-neighbor interactions governed by Rydberg blockade [92]. The MIS problem finds a set of the maximum number of vertices connected by edges. As an example of a 3-pan graph in Fig. 8(a), its MIS are  $\{\{1, 3\}, \{1, 4\}\}$ .

There are two challenges for the Rydberg-atom approach to solve combinatorial optimization problems. One is implementing large-scale graphs with complex connections, which requires arbitrary all-to-all couplings between vertices. The other is finding an efficient way to obtain the problem solutions. Embedding an arbitrary coupled graph is restricted because the maximum number of direct qubit connections is limited in a certain finite area and volume defined by the blockade radius  $r_b$  for two- and three-dimensional atomic structures, respectively. An effective connection between qubits physically separated farther than the blockade radius can be implemented by placing an auxiliary atomic chain (so-called Rydberg quantum wire) between them. Rydberg quantum wires realize all-to-all connections, including non-planar and high-degree graphs. The all-to-all connection can be implemented by demonstrating Kuratowski's subgraphs which are essential for embedding non-planar graphs [90]. Figure 8(b) shows an example to construct a non-planar  $K_{3,3}$  graph in a three-dimensional space, by placing three Rydberg quantum wires (red, yellow, and orange spheres) between the data qubit atoms (blue spheres)  $\{1, 4\}$ ,  $\{1, 6\}$ , and  $\{3, 4\}$ .

The quantum annealing method is an efficient way to find MIS problem solutions [93]. The MIS problem solutions are encoded to the ground states of the classical Ising Hamiltonian in Eq. (1) with  $\Omega = 0$  and  $0 < \Delta < U$ . By evolving the Hamiltonian from  $\Delta < 0$  and turning  $\Omega$  on and off, the MIS solution of the  $K_{3,3}$  graph  $\{\{1, 2, 3\}, \{4, 5, 6\}\}$  are obtained as frequently observed configurations out of  $2^6 = 64$  microstates in a probability histogram of Fig. 8(c). The detailed time strategy of the  $\Omega$  and  $\Delta$  during the quantum annealing can be modified by variational algorithms to optimize the answer obtaining performances. For example, an entire annealing path is divided into  $f$  segments, and a closed-loop optimization is conducted to find an optimal set of intermediate Hamiltonian parameters  $\Delta_i(t)$  and the duration of each segment  $\tau_i$ , as in Fig. 8(d). In Ref. [91], the variational quantum annealing algorithm is tested for various 80-vertices graphs with up to 8 degrees, and the performances are compared with simulated annealing (SA), a classical solution-finding algorithm, as in Fig. 8(e). The circuit depths (effective quantum annealing duration) showing minimum

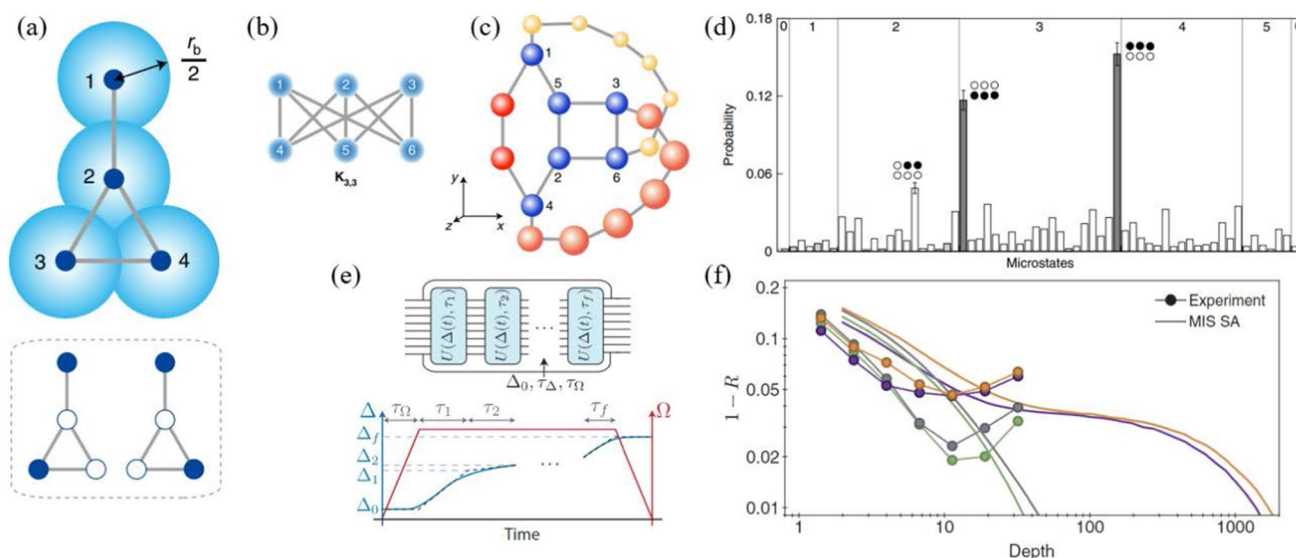


**Fig. 8** Graph implementations and maximum independent set (MIS) problems with Rydberg atom arrays. **a** A graph is implemented where vertices and edges are mapped from individual atoms and nearest-neighbor interactions. In an example 3-pan graph, the solutions of MIS problem are  $\{\{1, 3\}, \{1, 4\}\}$ . **b**  $K_{3,3}$  graph, which is one of Kuratowski's subgraphs. **c** Implementations of the  $K_{3,3}$  graph with Rydberg quantum wires. Three quantum wires of red, yellow, and orange spheres connects distant qubit atoms (blue spheres)  $\{1, 4\}$ ,

$\{1, 6\}$ , and  $\{3, 4\}$ , respectively. **d** A microstate probability shows the solutions of MIS problem of  $K_{3,3}$  are  $\{\{1, 2, 3\}, \{4, 5, 6\}\}$ . **e** A quantum variational algorithm to optimize the approximation ratio  $R$  of MIS solutions. **f** Comparing the performance of the quantum variational algorithm in experiments with simulated annealing (SA) for graphs with 80 vertices. **a–d** From [90]. **e–f** Reprinted figures from [91] with permission from AAAS

error ratio  $1 - R$  (defined by the average number of excitations) for the experiments are shorter than SA by more than two orders of magnitude.

## 4 Prospects

Up till now, the limit of the Rydberg quantum system size is about 250 atoms. The NP-complete problem's quantum advantage (the advantage of computational performance over digital computers) is expected to be achieved with about 5,000 atoms [92]. The currently developed and operated Rydberg quantum computers use alkali atoms (mainly Rubidium and Caesium), making it difficult to expand the system due to the intrinsic limitation of measurement efficiencies and decoherence [37, 94]. The next generation Rydberg quantum computers are being developed using alkali atoms in different environments, or using alkaline- or rare-earth atoms. In this section, we briefly review such newly developing platforms and technical efforts to improve the system performance, such as speed, scalability, stability, and controllability.

3D Rydberg atom arrays are already developed [31, 35] and would be merit in terms of scalability. But it also causes a drawback in fast image processing because of an additional dimension for the process. To reduce the processing cost, Ref. [95] devised a way to simultaneously

image fluorescence out of a three-dimensional array on a two-dimensional plane using a programmed SLM located in the quasi-Fourier domain between the Fourier and image planes. The method enables the three-dimensional imaging of an array aligned along the azimuthal axis using a tunable imaging lens [35], which is impossible by the conventional imaging method.

The finite trap lifetime is also a factor that limits the maximum number of atoms in a Rydberg array. Such a limited lifetime may be extended in a cryogenic environment because it lowers the level of the vacuum. In detail, the lifetime can be improved by a factor of 100 by increasing the vacuum level from the  $10^{-10}$  Torr, current level, to  $10^{-12}$  Torr, by lowering the environment temperature to liquid Helium 4 K with a pulse tube refrigerator. The experimental system with the cryogenic environment is described in Fig. 9(a). More than 300 atoms [96] are re-arrangement in this system, by achieving an effective lifetime of 6,000 s [97] in each optical dipole trap, where the low-temperature system is expected to increase the lifetime of the Rydberg states three times by reducing black-body-radiation (BBR) induced decays from Rydberg states.

Single species atoms are naturally identical and provide an advantage of scalability compared with artificial atoms (i.e., superconducting qubits). However, such identity also makes it difficult to locally address an atom without disturbing nearby atoms having the same resonance. In this regard,

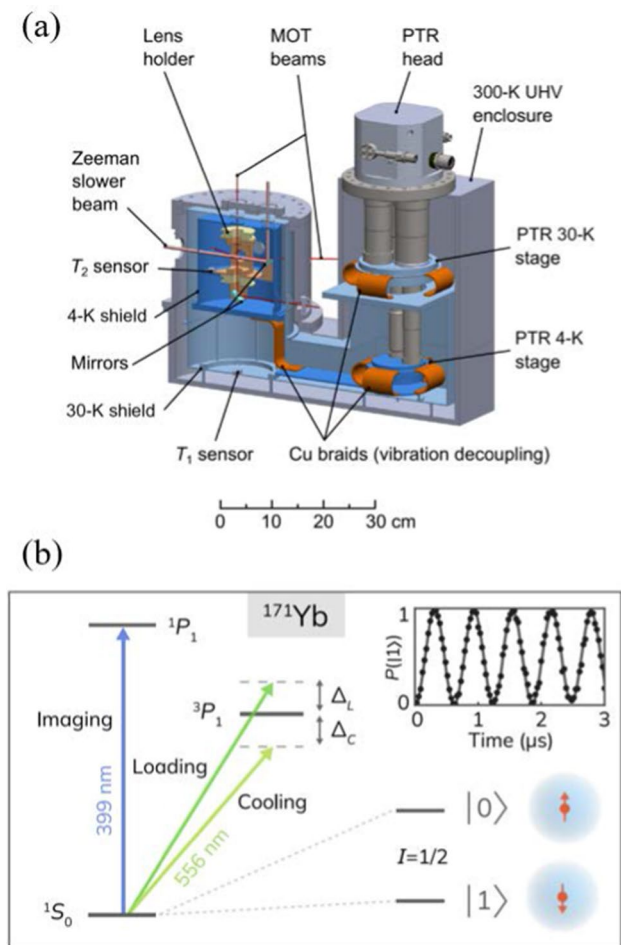


**Fig. 9** Currently developed trapped atomic platforms for the next generation. **a** Trapped atomic science chamber combined with a cryogenic system. Reprinted from [97] with permission. **b** The energy level of 171-Ytterbium atom. Reprinted from [107]

a dual-species atom array or heterogeneous isotopes were suggested for mid-circuit, non-demolition readout, and low crosstalk [98]. Rydberg-mediated entanglement between  $^{85}\text{Rb}$  and  $^{87}\text{Rb}$  has been demonstrated [99]. Recently, two-dimensional dual species arrays up to hundreds of or tens of atoms have also been generated for Rb-Cs [100] and  $^{85}\text{Rb}$ - $^{87}\text{Rb}$  [101]. Thus, the implementation of dual-species experiments would appear soon.

The divalent atomic elements, such as alkaline-earth and Ytterbium atoms, have been used in optical lattice clock platforms due to their stable transitions from richer energy structures. The next-generation Rydberg atom platforms are mainly developed based on these alkaline-earth-like atoms. The qubit-ground state  $|g\rangle$  of strontium-88 atoms can be mapped to one of the long-lived triplet state  $5s5p\ ^3P_0$ , which is prepared from the  $5s^2\ ^1S_0$  atomic ground state  $|a\rangle$  by the narrow-line width clock transition. Unlike the previous alkali-atom cases, the one-photon transition to the  $5s61s\ ^3S_1$

Rydberg state  $|r\rangle$  is conducted to eliminate additional dissipations to intermediate levels. The detection fidelity of the Rydberg state is also improved using a rapid auto-ionization process rather than the anti-trapping from the tweezer. The two-atom collective Rabi oscillation is obtained with long coherence of 60 cycles, and the high fidelity of Bell state 0.991(4) is recorded [102]. Other advantages, such as Rydberg trapping [103] and controllability by ion-core transitions [104], are also demonstrated, raising expectations for future development.

In the meantime, the alkaline-earth-like atom's ground state structure has no electronic orbital angular momentum that provides a different kind of qubit encoding than the standard hyperfine qubits of alkali atoms. Their fermionic elements have nearly degenerate ground states only from nuclear spin degrees of freedom. They are of weak sensitivity to a magnetic field and can have a long coherence time of over 10 s in dipole traps without dynamic decoupling thanks to small differential Stark shift [105]. Especially, nuclear spin 1/2 states of the metastable ground state of ytterbium-171 have attractive characteristics for quantum error corrections [106], so these are emerging as a new option for implementing neutral-atom quantum computing. Recent experiments demonstrated high fidelity single-qubit operations ( $F > 99.9\%$ ) for  $^{171}\text{Yb}$  nuclear spins in  $^1S_0$  ground state, by both fast Raman transition [107] and slow RF transition [108]. The relevant cooling transitions and an image of the trapped atomic array are shown in Fig. 9(b). Two-qubit entangling gate via Rydberg excitation is also demonstrated [108], showing its capability as a universal quantum processor.

## 5 Summary

In summary, Rydberg dipole blockade (entanglement techniques) and atom-arrangement techniques are the breakthrough technologies, triggering the latest progress in Rydberg quantum computing over the last decade. With the rapid development of the Rydberg platforms—such as large qubit numbers (scalability), coherence (stability), and defect-free rearrangements (controllability)—the Rydberg quantum computing community paves the way to quantum advantages. Rydberg quantum computers are hoped to be useful for classically difficult computations problems, such as logistics, production management, task management, and network design, as they seem to be best suitable for combinatorial optimization problems (traveler salesman problems, etc.). Consequently, start-up companies have recently been established to accelerate technology advancement and commercial use. Pasqal in France works with Browaeys's research team at Institut d'Optique to develop a Rydberg quantum computer using a two-dimensional rubidium atom

array to solve combinatorial optimization problems. Quera in the United States is working with Lukin's group at Harvard to improve the speed and fidelity of Rydberg quantum computers using about 200 rubidium atoms. Cold Quanta in the United States is a company that specializes in developing optical traps for Bose–Einstein condensation and has recently worked with Saffman's group at Univ. of Wisconsin to develop a circuit-based Rydberg quantum computing using a blue-detuned repulsive optical trap. Atom computing Inc. in the United States is developing a next-generation Rydberg quantum computer using alkaline-earth atoms in conjunction with NIST, the U.S. National Institute of Standards. Atom computing investigates the stabilization, automation, and development of new laser-driven technologies to improve the performance of Rydberg quantum computers. It might be interesting to see if the Rydberg quantum computing acts as a game changer in the existing quantum computing industry of superconducting qubits (IBM, Google, D-wave), ion-trapped qubits (IonQ, Quantinuum), and photons (Xanadu, PsiQuantum).

**Acknowledgements** This research was supported by Samsung Science and Technology Foundation (SSTF-BA1301-52). HJ acknowledges support from the Air Force Office of Scientific Research (FA2386-20-1-4068).

## References

- M.D. Lukin, M. Fleischhauer, R. Cote, L.M. Duan, D. Jaksch, J.I. Cirac, P. Zoller, Dipole blockade and quantum information processing in mesoscopic atomic ensembles. *Phys. Rev. Lett.* **87**, 037901 (2001)
- A. Gaëtan, Y. Miroshnychenko, T. Wilk, A. Chotia, M. Viteau, D. Comparat, P. Pillet, A. Browaeys, P. Grangier, Observation of collective excitation of two individual atoms in the Rydberg blockade regime. *Nat. Phys.* **5**, 115 (2009)
- E. Urban, T.A. Johnson, T. Henage, L. Isenhower, D.D. Yavuz, T.G. Walker, M. Saffman, Observation of Rydberg blockade between two atoms. *Nat. Phys.* **5**, 110 (2009)
- H. Kim, W. Lee, H. Lee, H. Jo, Y. Song, J. Ahn, In situ single-atom array synthesis using dynamic holographic optical tweezers. *Nat. Commun.* **7**, 13317 (2016)
- D. Barredo, S. de Léséleuc, V. Lienhard, T. Lahaye, A. Browaeys, An atom-by-atom assembler of defect-free arbitrary two-dimensional atomic arrays. *Science* **354**, 1021 (2016)
- M. Endres, H. Bernien, A. Keesling, H. Levine, E.R. Anschuetz, A. Krajenbrink, C. Senko, V. Vuletic, M. Greiner, M.D. Lukin, Atom-by-atom assembly of defect-free one-dimensional cold atom arrays. *Science* **354**, 6315, 1024 (2016)
- M. Saffman, T.G. Walker, K. Mølmer, Quantum information with Rydberg atoms. *Rev. Mod. Phys.* **82**, 2313 (2010)
- J. Lim, H. Lee, J. Ahn, Review of cold Rydberg atoms and their applications. *J. Kor. Phys. Soc.* **63**, 867 (2013)
- M. Saffman, Quantum computing with atomic qubits and Rydberg interactions: progress and challenges. *J. Phys. B* **49**, 202001 (2016)
- A. Browaeys, T. Lahaye, Many-body physics with individually controlled Rydberg atoms. *Nat. Phys.* **16**, 132 (2020)
- M. Morgado, S. Whitlock, Quantum simulation and computing with Rydberg-interacting qubits. *AVS Quantum Sci.* **3**, 023501 (2021)
- X. Wu, X. Liang, Y. Tian, F. Yang, C. Chen, Y.-C. Liu, M.K. Tey, L. You, A concise review of Rydberg atom based quantum computation and quantum simulation. *Chin. Phys. B* **30**, 020305 (2021)
- R. Grimm, M. Weidemüller, Y.B. Ovchinnikov, Optical dipole traps for neutral atoms. *Adv. At. Mol. Opt. Phys.* **42**, 95 (2000)
- N. Schlosser, G. Reymond, I. Protsenko, P. Grangier, Sub-poissonian loading of single atoms in a microscopic dipole trap. *Nature* **411**, 1024 (2001)
- F. Nogrette, H. Labuhn, S. Ravets, D. Barredo, L. Béguin, A. Vernier, T. Lahaye, A. Browaeys, Single-atom trapping in holographic 2D arrays of microtraps with arbitrary geometries. *Phys. Rev. X* **4**, 021034 (2014)
- D.O. Mello, D. Schäffner, J. Werkmann, T. Preuschoff, L. Kohfahl, M. Schlosser, G. Birkel, Defect-free assembly of 2D clusters of more than 100 single-atom quantum systems. *Phys. Rev. Lett.* **122**, 203601 (2019)
- M.J. Piotrowicz, M. Lichtman, K. Maller, G. Li, S. Zhang, L. Isenhower, M. Saffman, Two-dimensional lattice of blue-detuned atom traps using a projected Gaussian beam array. *Phys. Rev. A* **88**, 013420 (2013)
- P. Xu, X. He, J. Wang, M. Zhan, Trapping a single atom in a blue detuned optical bottle beam trap. *Opt. Lett.* **35**, 2164 (2010)
- Y.R.P. Sortais, H. Marion, C. Tuchendler, A.M. Lance, M. Lamare, P. Fournet, C. Armellin, R. Mercier, G. Messin, A. Browaeys, P. Grangier, Diffraction-limited optics for single-atom manipulation. *Phys. Rev. A* **75**, 013406 (2007)
- S.K. Dutta, J.R. Guest, D. Feldbaum, A. Walz-Flannigan, G. Raithel, Ponderomotive optical lattice for Rydberg atoms. *Phys. Rev. Lett.* **85**, 5551 (2000)
- S. Zhang, F. Robicheaux, M. Saffman, Magic-wavelength optical traps for Rydberg atoms. *Phys. Rev. A* **84**, 043408 (2011)
- D. Barredo, V. Lienhard, P. Scholl, S. de Léséleuc, T. Boulier, A. Browaeys, T. Lahaye, Three-dimensional trapping of individual Rydberg atoms in ponderomotive bottle beam traps. *Phys. Rev. Lett.* **124**, 023201 (2020)
- P. Huft, Y. Song, T.M. Graham, K. Jooya, S. Deshpande, C. Fang, M. Kats, M. Saffman, Simple, passive design for large optical trap arrays for single atoms. *Phys. Rev. A* **105**, 063111 (2022)
- N. Schlosser, G. Reymond, P. Grangier, Collisional blockade in microscopic optical dipole traps. *Phys. Rev. Lett.* **89**, 023005 (2002)
- T. Cizmar, M. Mazilu, K. Dholakia, In situ wavefront correction and its application to micromanipulation. *Nat. Photon.* **4**, 388 (2010)
- M. Persson, D. Engstrom, M. Goksor, Reducing the effect of pixel crosstalk in phase only spatial light modulators. *Opt. Express* **20**, 22334 (2012)
- H. Tamura, T. Unakami, J. He, Y. Miyamoto, K. Nakagawa, Highly uniform holographic microtrap arrays for single atom trapping using a feedback optimization of in-trap fluorescence measurements. *Opt. Express* **24**, 8132 (2016)
- D. Kim et al., Large-scale uniform optical focus array generation with a phase spatial light modulator. *Opt. Lett.* **44**, 3178 (2019)
- W. Lee, H. Kim, J. Ahn, Defect-free atomic array formation using the Hungarian matching algorithm. *Phys. Rev. A* **95**, 053424 (2017)
- H. Kim, M. Kim, W. Lee, J. Ahn, Gerchberg-Saxton algorithm for tweezer-trap atom arrangements. *Opt. Express* **27**(3), 2184 (2019)
- W. Lee, H. Kim, J. Ahn, Three-dimensional rearrangement of single atoms using actively controlled optical microtraps. *Opt. Express* **24**, 9816 (2016)

32. K.-N. Schymik, V. Lienhard, D. Barredo, P. Scholl, H. Williams, A. Browaeys, T. Lahaye, Enhanced atom-by-atom assembly of arbitrary tweezer arrays. *Phys. Rev. A* **102**, 063107 (2020)
33. C. Sheng, J. Hou, X. He, P. Xu, K. Wang, J. Zhuang, X. Li, M. Liu, J. Wang, M. Zhan, Efficient preparation of two-dimensional defect-free atom arrays with near-fewest sorting-atom moves. *Phys. Rev. Res.* **3**, 023008 (2021)
34. S. Ebadi, T.T. Wang, H. Levine, A. Keesling, G. Semeghini, A. Omran, D. Bluvstein, R. Samajdar, H. Pichler, W.W. Ho, S. Choi, S. Sachdev, M. Greiner, V. Vuletić, M.D. Lukin, Quantum phases of matter on a 256-atom programmable quantum simulator. *Nature* **595**, 227 (2021)
35. V. Lienhard, S. de Léséleuc, T. Lahaye, A. Browaeys, Synthetic three-dimensional atomic structures assembled atom by atom. *Nature* **561**, 79 (2018)
36. Y. Miroshnychenko, A. Gaëtan, C. Evellin, P. Grangier, D. Comparat, P. Pillet, T. Wilk, A. Browaeys, Coherent excitation of a single atom to a Rydberg state. *Phys. Rev. A* **82**, 013405 (2010)
37. S. de Léséleuc, D. Barredo, V. Lienhard, A. Browaeys, T. Lahaye, Analysis of imperfections in the coherent optical excitation of single atoms to Rydberg states. *Phys. Rev. A* **97**, 053803 (2018)
38. H. Levine, A.R. Keesling, A. Omran, H. Bernien, S. Schwartz, A.S. Zibrov, M. Endres, M. Greiner, V. Vuletić, M.D. Lukin, High-fidelity control and entanglement of Rydberg-atom qubits. *Phys. Rev. Lett.* **121**, 123603 (2018)
39. T.M. Graham, M. Kwon, B. Grinkemeyer, Z. Marra, X. Jian, M.T. Lichtman, Y. Sun, M. Ebert, M. Saffman, Rydberg-mediated entanglement in a two-dimensional neutral atom qubit array. *Phys. Rev. Lett.* **123**, 230501 (2019)
40. T. Wilk, A. Gaëtan, C. Evellin, J. Wolters, Y. Miroshnychenko, P. Grangier, A. Browaeys, Entanglement of two individual neutral atoms using Rydberg blockade. *Phys. Rev. Lett.* **104**, 010502 (2010)
41. S. Kuhr, W. Alt, D. Schrader, I. Dotsenko, Y. Miroshnychenko, W. Rosenfeld, M. Khudaverdyan, V. Gomer, A. Rauschenbeutel, D. Meschede, Coherence properties and quantum state transportation in an optical conveyor belt. *Phys. Rev. Lett.* **91**, 213002 (2003)
42. M. Martinez-Dorantes, W. Alt, J. Gallego, S. Ghosh, L. Ratschbacher, Y. Völzke, D. Meschede, Fast nondestructive parallel readout of neutral atom registers in optical potentials. *Phys. Rev. Lett.* **119**, 180503 (2017)
43. M. Kwon, M.F. Ebert, T.G. Walker, M. Saffman, Parallel low-loss measurement of multiple atomic qubits. *Phys. Rev. Lett.* **119**, 180504 (2017)
44. S. Ravets, H. Labuhn, D. Barredo, L. Béguin, T. Lahaye, A. Browaeys, Coherent dipole-dipole coupling between two single Rydberg atoms at an electrically-tuned Förster resonance. *Nat. Phys.* **10**, 914 (2014)
45. D. Jaksch, J.I. Cirac, P. Zoller, S.L. Rolston, R. Côté, M.D. Lukin, Fast quantum gates for neutral atoms. *Phys. Rev. Lett.* **85**, 2208 (2000)
46. L. Isenhower, E. Urban, X.L. Zhang, A.T. Gill, T. Henage, T.A. Johnson, T.G. Walker, M. Saffman, Demonstration of a neutral atom controlled-NOT quantum gate. *Phys. Rev. Lett.* **104**, 010503 (2010)
47. M. Ebert, A. Gill, M. Gibbons, X. Zhang, M. Saffman, T.G. Walker, Atomic Fock state preparation using Rydberg blockade. *Phys. Rev. Lett.* **112**, 043602 (2014)
48. Y.-Y. Jau, A.M. Hankin, T. Keating, I.H. Deutsch, G.W. Biedermann, Entangling atomic spins with a Rydberg dressed spin-flip blockade. *Nat. Phys.* **12**, 71 (2015)
49. H. Jo, Y. Song, M. Kim, J. Ahn, Rydberg atom entanglements in the weak coupling regime. *Phys. Rev. Lett.* **124**, 033603 (2020)
50. A. Omran et al., Generation and manipulation of Schrödinger cat states in Rydberg atom arrays. *Science* **365**, 6453, 570 (2019)
51. X.-L. Wang, J.-W. Pan et al., 18-qubit entanglement with six photons' three degrees of freedom. *Phys. Rev. Lett.* **120**, 260502 (2018)
52. T. Monz, R. Blatt et al., 14-qubit entanglement: creation and coherence. *Phys. Rev. Lett.* **106**, 130506 (2011)
53. C. Song, K. Xu, H. Li, H. Fan, D. Zheng, H. Wang et al., Generation of multicomponent atomic Schrödinger cat states of up to 20 qubits. *Science* **365**, 574 (2019)
54. T. Xia, M. Lichtman, K. Maller, A.W. Carr, M.J. Piotrowicz, L. Isenhower, M. Saffman, Randomized benchmarking of single-qubit gates in a 2D array of neutral-atom qubits. *Phys. Rev. Lett.* **114**, 100503 (2015)
55. Y. Wang, A. Kumar, T.-Y. Wu, D.S. Weiss, Single-qubit gates based on targeted phase shifts in a 3D neutral atom array. *Science* **352**, 1562 (2016)
56. Y. Song, J. Lim, J. Ahn, Berry-phase gates for fast and robust control of atomic clock states. *Phys. Rev. Res.* **2**, 023045 (2020)
57. H. Levine, D. Bluvstein, A. Keesling, T.T. Wang, S. Ebadi, G. Semeghini, A. Omran, M. Greiner, V. Vuletić, M.D. Lukin, Dispersive optical systems for scalable Raman driving of hyperfine qubits. *Phys. Rev. A* **105**, 032618 (2022)
58. H. Levine, A. Keesling, G. Semeghini, A. Omran, T.T. Wang, S. Ebadi, H. Bernien, M. Greiner, V. Vuletić, H. Pichler, M.D. Lukin, Parallel implementation of high-fidelity multiqubit gates with neutral atoms. *Phys. Rev. Lett.* **123**, 170503 (2019)
59. Y. Sun, P. Xu, Controlled phase gate protocol for neutral atoms via off-resonant modulated driving. *Phys. Rev. Appl.* **13**, 024059 (2020)
60. F. Robicheaux, T.M. Graham, M. Saffman, Photon-recoil and laser-focusing limits to Rydberg gate fidelity. *Phys. Rev. A* **103**, 022424 (2021)
61. A. Pagano, S. Weber, D. Jaschke, T. Pfau, F. Meinert, S. Montanero, H.P. Büchler, Error budgeting for a controlled-phase gate with strontium-88 Rydberg atoms. *Phys. Rev. Res.* **4**, 033019 (2022)
62. Z. Fu, P. Xu, Y. Sun, Y.-Y. Liu, X.-D. He, X. Li, M. Liu, R.-B. Li, J. Wang, L. Liu, M.-S. Zhan, High-fidelity entanglement of neutral atoms via a Rydberg-mediated single-modulated-pulse controlled-phase gate. *Phys. Rev. A* **105**, 042430 (2022)
63. D. Bluvstein, H. Levine, G. Semeghini, T.T. Wang et al., A quantum processor based on coherent transport of entangled atom arrays. *Nature* **604**, 451 (2022)
64. T.M. Graham, Y. Song, M. Saffman et al., Multi-qubit entanglement and algorithms on a neutral-atom quantum computer. *Nature* **604**, 457 (2022)
65. I.M. Georgescu, S. Ashhab, F. Nori, Quantum simulation. *Rev. Mod. Phys.* **86**, 153 (2014)
66. E. Altman et al., Quantum simulators: architectures and opportunities. *PRX Quantum* **2**, 017003 (2021)
67. H. Labuhn, D. Barredo, S. Ravets, S. de Léséleuc, T. Macrì, T. Lahaye, A. Browaeys, Tunable two-dimensional arrays of single Rydberg atoms for realizing quantum Ising models. *Nature* **534**, 667–670 (2016)
68. L. Béguin, A. Vernier, R. Chicireanu, T. Lahaye, A. Browaeys, Direct measurement of the van der Waals interaction between two Rydberg atoms. *Phys. Rev. Lett.* **110**, 263201 (2013)
69. M. Kim, Y. Song, J. Kim, J. Ahn, Quantum Ising hamiltonian programming in trio, quartet, and sextet qubit systems. *PRX Quantum* **1**, 020323 (2020)
70. H. Kim, Y. Park, K. Kim, H.-S. Sim, J. Ahn, Detailed balance of thermalization dynamics in Rydberg atom quantum simulators. *Phys. Rev. Lett.* **120**, 180502 (2018)
71. S. Sachdev, Quantum magnetism and criticality. *Nat. Phys.* **4**, 173–185 (2008)
72. H. Bernien, S. Schwartz, A. Keesling, H. Levine, A. Omran, H. Pichler, S. Choi, A.S. Zibrov, M. Endres, M. Greiner, V. Vuletić,

- M.D. Lukin, Probing many-body dynamics on a 51-atom quantum simulator. *Nature* **551**, 579–584 (2017)
73. V. Lienhard, S. de Léséleuc, D. Barredo, T. Lahaye, A. Browaeys, M. Schuler, L.P. Henry, A.M. Läuchli, Observing the space- and time-dependent growth of correlations in dynamically tuned synthetic Ising models with antiferromagnetic interactions. *Phys. Rev. X* **8**, 021070 (2018)
  74. P. Scholl, M. Schuler, H.J. Williams, A.A. Eberharter, D. Barredo, K.N. Schymik, V. Lienhard, L.P. Henry, T.C. Lang, T. Lahaye, A.M. Läuchli, A. Browaeys, Quantum simulation of 2D antiferromagnets with hundreds of Rydberg atoms. *Nature* **595**, 233 (2021)
  75. Y. Song, M. Kim, H. Hwang, W. Lee, J. Ahn, Quantum simulation of Cayley-tree Ising Hamiltonians with three-dimensional Rydberg atoms. *Phys. Rev. Res.* **3**, 013286 (2021)
  76. A. Keesling, A. Omran, H. Levine, H. Bernien, H. Pichler, S. Choi, R. Samajdar, S. Schwartz, P. Silvi, S. Sachdev, P. Zoller, M. Endres, M. Greiner, V. Vuletić, M.D. Lukin, Quantum Kibble-Zurek mechanism and critical dynamics on a programmable Rydberg simulator. *Nature* **568**, 207 (2019)
  77. G. Semeghini, A. Vishwanath, M. Greiner, V. Vuletic, M.D. Lukin et al., Probing topological spin liquids on a programmable quantum simulator. *Science* **374**, 1242 (2021)
  78. L. Savary, L. Balents, Quantum spin liquids: a review. *Rep. Prog. Phys.* **80**, 016502 (2016)
  79. A. Kitaev, Fault-tolerant quantum computation by anyons. *Ann. Phys.* **303**, 2 (2003)
  80. J. Eisert, M. Friesdorf, C. Gogolin, Quantum many-body systems out of equilibrium. *Nat. Phys.* **11**, 124 (2015)
  81. D.A. Abanin, E. Altman, I. Bloch, M. Serbyn, Colloquium: Many-body localization, thermalization, and entanglement. *Rev. Mod. Phys.* **91**, 021001 (2019)
  82. S. Moudgalya, B.A. Bernevig, N. Regnault, Quantum many-body scars and Hilbert space fragmentation: a review of exact results. *Rep. Prog. Phys.* **85**, 086501 (2022)
  83. D. Bluvstein, A. Omran, H. Levine, A. Keesling, G. Semeghini, S. Ebadi, T.T. Wang, A.A. Michailidis, N. Maskara, W.W. Ho, S. Choi, M. Serbyn, M. Greiner, V. Vuletić, M.D. Lukin, Controlling quantum many-body dynamics in driven Rydberg atom arrays. *Science* **371**, 1355 (2021)
  84. D.V. Else, C. Monroe, C. Nayak, N.Y. Yao, Discrete time crystals. *Annu. Rev. Cond. Mat. Phys.* **11**, 467 (2020)
  85. D. Barredo, H. Labuhn, S. Ravets, T. Lahaye, A. Browaeys, C.S. Adams, Coherent excitation transfer in a spin chain of three Rydberg atoms. *Phys. Rev. Lett.* **114**, 113002 (2015)
  86. S. de Léséleuc, D. Barredo, V. Lienhard, A. Browaeys, T. Lahaye, Optical control of the resonant dipole-dipole interaction between Rydberg atoms. *Phys. Rev. Lett.* **119**, 053202 (2017)
  87. S. de Léséleuc, V. Lienhard, P. Scholl, D. Barredo, S. Weber, N. Lang, H.P. Büchler, T. Lahaye, A. Browaeys, Observation of a symmetry-protected topological phase of interacting bosons with Rydberg atoms. *Science* **365**, 775 (2019)
  88. P. Scholl, H.J. Williams, G. Bornet, F. Wallner, D. Barredo, L. Henriot, A. Signoles, C. Hainaut, T. Franz, S. Geier, A. Tebben, A. Salzinger, G. Zürn, T. Lahaye, M. Weidemüller, A. Browaeys, Microwave engineering of programmable XXZ Hamiltonians in arrays of Rydberg atoms. *PRX Quantum* **3**, 020303 (2022)
  89. H. Pichler, S.-T. Wang, L. Zhou, S. Choi, and M. D. Lukin, Quantum optimization for maximum independent set using Rydberg atom arrays, [arXiv: 1808.10816](https://arxiv.org/abs/1808.10816)
  90. M. Kim, K. Kim, J. Hwang, E.-G. Moon, J. Ahn, Rydberg quantum wires for maximum independent set problems. *Nat. Phys.* **18**, 755 (2022)
  91. S. Ebadi, A. Keesling, M. Cain, T.T. Wang et al., Quantum optimization of maximum independent set using Rydberg atom arrays. *Science* **376**, 1209 (2022)
  92. M.F. Serret, B. Marchand, T. Ayril, Solving optimization problems with Rydberg analog quantum computers: Realistic requirements for quantum advantage using noisy simulation and classical benchmarks. *Phys. Rev. A* **102**, 052617 (2020)
  93. T. Albash, D.A. Lidar, Adiabatic quantum computation. *Rev. Mod. Phys.* **90**, 015002 (2018)
  94. W. Lee, M. Kim, H. Jo, Y. Song, Coherent and dissipative dynamics of entangled few-body systems of Rydberg atoms. *Phys. Rev. A* **99**, 043404 (2019)
  95. H. Sun, Y. Song, A. Byun, H. Jeong, J. Ahn, Imaging three-dimensional single-atom arrays all at once. *Opt. Express* **29**, 4082 (2021)
  96. K.-N. Schymik, B. Ximenez, E. Bloch, D. Dreon, A. Signoles, F. Nogrette, D. Barredo, A. Browaeys, T. Lahaye, In situ equalization of single-atom loading in large-scale optical tweezer arrays. *Phys. Rev. A* **106**, 022611 (2022)
  97. K.-N. Schymik, A. Browaeys et al., Single atoms with 6000-second trapping lifetimes in optical-tweezer arrays at cryogenic temperatures. *Phys. Rev. Appl.* **16**, 034013 (2021)
  98. I.I. Beterov, M. Saffman, Rydberg blockade, Forster resonances, and quantum state measurements with different atomic species. *Phys. Rev. A* **92**, 042710 (2015)
  99. Y. Zeng, P. Xu, X. He, Y. Liu, M. Liu, J. Wang, D.J. Papoular, G.V. Shlyapnikov, M. Zhan, Entangling two individual atoms of different isotopes via Rydberg blockade. *Phys. Rev. Lett.* **119**, 160502 (2017)
  100. K. Singh, S. Anand, A. Pocklington, J.T. Kemp, H. Bernien, Dual-element, two-dimensional atom array with continuous-mode operation. *Phys. Rev. X* **12**, 011040 (2022)
  101. C. Sheng, J. Hou, X. He, K. Wang, R. Guo, J. Zhuang, B. Mamat, P. Xu, J. Wang, Liu, M. Zhan, Defect-free arbitrary-geometry assembly of mixed-species atom arrays. *Phys. Rev. Lett.* **128**, 083202 (2022)
  102. I.S. Madjarov, J.P. Covey, A.L. Shaw, J. Choi, A. Kale, A. Cooper, H. Pichler, V. Schkolnik, J.R. Williams, M. Endres, High-fidelity entanglement and detection of alkaline-earth Rydberg atoms. *Nat. Phys.* **16**, 857 (2020)
  103. J.T. Wilson, S. Saskin, Y. Meng, S. Ma, R. Dilip, A.P. Burgers, J.D. Thompson, Trapping alkaline earth Rydberg atoms optical tweezer arrays. *Phys. Rev. Lett.* **128**, 033201 (2022)
  104. A.P. Burgers, S. Ma, S. Saskin, J. Wilson, M.A. Alarcón, C.H. Greene, J.D. Thompson, Controlling Rydberg excitations using ion-core transitions in alkaline-earth atom-tweezer arrays. *PRX Quantum* **3**, 020326 (2022)
  105. K. Barnes, B.J. Bloom, K. Kotru, M. McDonald et al., Assembly and coherent control of a register of nuclear spin qubits. *Nat. Commun.* **13**, 2779 (2022)
  106. Y. Wu, S. Kolkowitz, S. Puri, J.D. Thompson, Erasure conversion for fault-tolerant quantum computing in alkaline earth Rydberg atom arrays. *Nat. Commun.* **13**, 4657 (2022)
  107. A. Jenkins, J.W. Lis, A. Senoo, W.F. McGrew, A.M. Kaufman, Ytterbium nuclear-spin qubits in an optical tweezer array. *Phys. Rev. X* **12**, 021027 (2022)
  108. S. Ma, Alex P. Burgers, G. Liu, J. Wilson, B. Zhang, J.D. Thompson, Universal gate operations on nuclear spin qubits in an optical tweezer array of 171Yb atoms. *Phys. Rev. X* **12**, 021028 (2022)

**Publisher's Note** Springer Nature remains neutral with regard to jurisdictional claims in published maps and institutional affiliations.

Springer Nature or its licensor (e.g. a society or other partner) holds exclusive rights to this article under a publishing agreement with the author(s) or other rightsholder(s); author self-archiving of the accepted manuscript version of this article is solely governed by the terms of such publishing agreement and applicable law.